IChemE

www.icheme.org/journals
doi: 10.1205/cherd.03401

0263–8762/05/$30.00+0.00

Trans IChemE, Part A, April 2005
Chemical Engineering Research and Design, 83(A4): 357–371

FLUID MECHANICS AND DESIGN ASPECTS OF A NOVEL OSCILLATORY FLOW SCREENING MESOREACTOR

N. REIS[1], A. P. HARVEY[3,*], M. R. MACKLEY[2], A. A. VICENTE[1] and J. A. TEIXEIRA[1]

[1]*Centro de Engenharia Biológica, Universidade do Minho, Braga, Portugal*
[2]*Department of Chemical Engineering, University of Cambridge, Cambridge, UK*
[3]*School of Chemical Engineering and Advanced Materials, University of Newcastle upon Tyne, UK*

A novel, continuous, oscillatory flow screening mesoreactor, composed of tubes with smooth periodic constrictions, is presented as a new option for small-scale reaction engineering applications, particularly those involving the screening of solid catalysts. Experimental studies using particle image velocimetry have demonstrated that this reactor provides good fluid mixing, and is able to suspend catalyst particles with a wide range of sedimentation velocities. Results from 2D and 3D CFD simulations exhibit semi-quantitative agreement with the experimental data, and will aid in the design of future reactors. Potential application areas for this reactor are specialist chemical manufacture and high-throughput screening. Unlike conventional screening devices, the flow patterns in this reactor can be reproduced at larger scales, therefore, results in the laboratory can be related directly to larger scale production.

Keywords: continuous screening reactor; CFD; PIV; oscillatory flow; screening; catalyst particle suspension.

INTRODUCTION

Since the early 1990s, studies have shown that tubes containing periodically-spaced orifice baffles, when subjected to a net flow with a reversing oscillatory component of the correct magnitude, can exhibit efficient fluid mixing and a narrow residence time distribution (Brunold *et al.*, 1989; Dickens *et al.*, 1989; Howes *et al.*, 1991; Mackley and Ni, 1991, 1993; Stonestreet and van der Veeken, 1999). The baffle edges promote eddy formation, which increases the radial mixing in the tube, leading to radial velocities of the same order of magnitude as the axial velocities (e.g., Mackley, 1991; Mackley and Ni, 1991; Ni and Pereira, 2000). These 'oscillatory flow reactors' (OFRs) can be operated continuously in horizontal or vertical tubes containing liquid or multiphase flows. The fluid is oscillated in the axial direction by means of diaphragms, bellows or pistons, at one or both ends of the tube, or by moving a set of baffles up and down from the top of the tube (Ni *et al.*, 2002).

The efficiency of the radial transport is affected by many variables, such as the oscillation frequency (f), amplitude (x_0), reactor internal diameter (d), baffle spacing (L), baffle internal diameter (d_0), baffle thickness (δ), the fluid's rheological properties (density, ρ, and viscosity, μ) and the net flow Reynolds number (Re_n). The intensity of mixing in an OFR is commonly described by the oscillatory Reynolds number, Re_o, and the Strouhal number St_r, which are defined as (Ni and Gough, 1997):

$$Re_o = \frac{2\pi f x_0 \rho d}{\mu} \tag{1}$$

$$St_r = \frac{d}{4\pi x_0} \tag{2}$$

At Re_o values of 100–300, vortex rings are symmetrically generated within each baffle cavity during each oscillation of the fluid. At higher Re_os, the flow becomes more intensely mixed and chaotic, leading to increased axial mixing such that the OFR's mixing increasingly resembles that of a stirred tank (Ni *et al.*, 1999, 2002). The generation of vortices is no longer axi-symmetrical (Ni *et al.*, 2002). These phenomena remain the same between reactors of different diameters, indicating that the fluid mechanical conditions in an OFR can be linearly scaled up (Brunold *et al.*, 1989; Dickens *et al.*, 1989; Ni *et al.*, 1995b). The fluid mechanics of OFRs at millimetre scales, however, have not previously been studied.

Experiments by Smith (1993) and flow visualization studies by Ni *et al.* (1995a) show that fluid oscillation in an OFR is an efficient method of uniformly suspending

*Correspondence to: Dr A. P. Harvey, School of Chemical Engineering and Advanced Materials, University of Newcastle upon Tyne, Merz Court, Newcastle upon Tyne, NE1 7RU, UK.
E-mail: a.p.harvey@ncl.ac.uk

particles. The performance of the OFR as a heterogeneous catalytic reactor has been demonstrated for the suspension of titania particles acting as catalysts to oxidise waste water contaminants (Fabiyi and Skelton, 2000). The OFR has also been shown to be an effective particle separator (Mackley *et al.*, 1993).

The formation and dissipation of eddies in the OFR results in significant enhancement of processes such as heat transfer (Mackley *et al.*, 1990; Mackley and Stonestreet, 1995), mass transfer (Hewgill *et al.*, 1993; Ni *et al.*, 1995a, b; Ni and Gao, 1996), particle mixing and separation (Mackley *et al.*, 1993), liquid–liquid reaction (Ni and Mackley, 1993), polymerization (Ni *et al.*, 1998, 1999) and flocculation (Gao *et al.*, 1998). The OFR increases the hold-up time of bubbles and particles, and is an effective method of controlling drop and bubble size distributions. Other phenomena that have been investigated in the OFR include: its fluid mechanics (Brunold *et al.*, 1989; Mackley and Ni, 1991, 1993), local velocity profiles and shear rate distribution (Ni *et al.*, 1995c), residence time distribution (Dickens *et al.*, 1989; Mackley and Ni, 1991, 1993; Ni, 1994), dispersion (Howes, 1988; Howes and Mackley, 1990), velocity profiles (Liu *et al.*, 1995) and scale-up correlations (Ni and Gao, 1996). A full review of the applications of oscillatory flow technology is presented in Baird *et al.* (2003).

This paper describes the evaluation of a novel, oscillatory flow screening mesoreactor, using particle image velocimetry (PIV), combined with computational fluid dynamics (CFD). The scale of this novel reactor is smaller than that used before and the geometry includes smooth periodic constrictions, rather than sharp-edged baffles.

MATERIALS AND METHODS

The Screening Reactor

The fundamental unit of the screening mesoreactor is a 35 cm long, 4.4 mm internal diameter glass jacketed tube as shown in Figure 1.

The inner tube has smooth periodic constrictions (SPCs), of mean spacing 13 mm (approximately 3*d*) and a constriction length of 6 mm. The diameter of the constricted zone was 1.6 mm, representing 13% of the cross-sectional area. It should be noted that this is considerably less than the 50% open cross-sectional area used in conventional OFRs. Another important difference is that the constrictions are smooth, rather than sharp: this is intended to reduce high shear regions, such as those found at the edge of sharp baffles, thereby making the device amenable to bioprocessing applications.

In these trials a single smooth periodic constricted (SPC) tube was usually positioned vertically, and the fluid oscillated using a piston fitted on an electromagnetic oscillator, connected to the base of the tube by means of a 5 mm internal diameter PVC tube. A signal generator and amplifier controlled the piston oscillation frequency and amplitude. Fluid oscillation frequencies between 0 and 50 Hz and amplitudes between 0 and 20 mm (centre-to-peak) were possible, but the apparatus could not provide both high frequency and high amplitude. The fluid oscillation amplitude was monitored by reading the liquid level in a 2.0 mm internal diameter scaled glass tube, connected to the top of the SPC tube, the smaller internal diameter of the measuring tube increasing the resolution of amplitude measurement approximately tenfold. The fluid used was tap water at room temperature (20°C), pumped into the

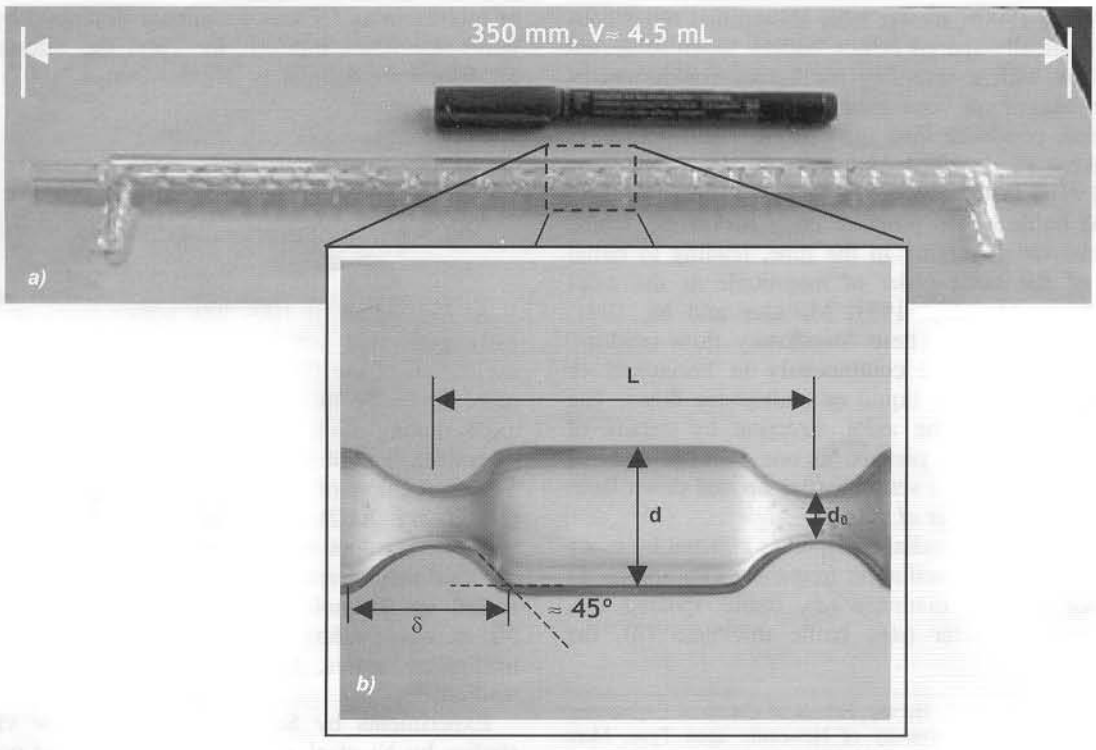

Figure 1. Geometry of a single SPC tube.

reactor using a peristaltic pump connected to the bottom of the reactor via a nonreturn valve. All experiments were conducted in batch mode.

Particle Image Velocimetry Apparatus

In order to minimize optical distortion, a rectangular Perspex optical box was fitted around the centre of the reactor tube and filled with glycerol (which has a refractive index similar to Perspex and glass). The glass jacket of the reactor tube was also filled with glycerol. The light source was a Nd:YAG dual pulsed laser, with a wavelength of 532 nm and a maximum power intensity of 40 mJ. The beam was diverged into a vertical light sheet, ~1 mm thick, and positioned to cross the middle of the flow field.

A CCD camera (1000 × 1200 pixels, PCO Sensicam) was located perpendicularly to the laser sheet. As the camera used was limited to low image acquisition frequencies (1–4 Hz), a phase difference of 0.1 Hz was imposed between the frequencies of camera capture and oscillator unit to obtain the velocity profiles at different piston positions. This allowed 10 equally spaced phase images per cycle. The phase angle of a picture was determined by either reading the level meter captured at the same moment with a second digital camera, or by analysis of the average axial velocity profile. The cameras were synchronized with the laser source using an ILA synchronizer (ILA, Juelich, Germany). The reactor was seeded with neutrally buoyant silvered 'microspheres' with a mean particle diameter of 10 μm, at a seeding to liquid ratio of 10^{-5}:1, as recommended by Elgobashi (1994). The seeded fluid was oscillated for 5 min before image acquisition was initiated, to ensure that the seeding was well-dispersed. All experiments were performed at room temperature (*ca.* 20°C).

The results were processed using VidPIV® software (ILA, Juelich, Germany) and plotted using TECPLOT® software. In each experiment 30 images were acquired, permitting three equal phase images for each phase angle. The instantaneous velocity vector maps were constructed for each image, as well as averaged maps for each phase angle. Experiments were carried out at fifteen amplitude-frequency combinations, corresponding to Re_o values between 12 and 1335, covering the expected axisymmetric and nonaxisymmetric regimes (Mackley and Ni, 1991; Mackley, 1990; Howes *et al.*, 1991).

The following conditions were used, to provide a wide range of Re_os, as well as to investigate the effects of both amplitude and frequency individually Table 1:

Two further series of experiments were performed to investigate the effect of gravity on the fluid mechanics and particle suspensions: at oscillation frequencies of (i) 4.1 Hz and (ii) 12.1 Hz and fluid amplitudes between 3 and 4 mm, the reactor was positioned at 90°, 45° or 10° to the horizontal.

Computational Fluid Dynamics

The CFD package used was 'Fluent' 5.5 (1998). Meshes were created using Gambit 1.2.2 software. In Fluent, the velocity profiles in the inlet and outlet of the SPC had to be matched. This condition was imposed on 'Fluent' by using periodic boundary conditions, but it should be noted that such conditions can only be used if the number and location of nodes is similar in both periodic zones (inlet and outlet). 2D planar, 2D with axisymmetric and 3D meshes were constructed and used to simulate flow patterns within the SPC tube. Firstly, mesh size independency was studied for the 2D planar model at continuous flow. Then, 2D axisymmetric and 3D geometries were meshed using the minimum cell size required for mesh independency of the results (from the 2D planar results), so that computational times were minimized. The number of cells were 6820 and 110,772, respectively. The grid used in 3D simulations is presented in Figure 2. Details of the meshing can be found in Table 2.

Table 1. Experimental conditions.

Amplitude (mm)	Frequency (Hz)	Oscillatory Re_o (-)
0.2	2.1	12
0.3	2.1	17
1	4.1	113
1	5.1	141
1	10.1	279
1	11.1	307
1	15.1	417
1	20.1	556
3	2.1	174
5	2.1	290
4	1.1	122
11	1.1	335

For continuous flow, the mean flow velocity was specified as a constant and set as one of the 'Fluent' boundary conditions. For oscillatory flow, the displacement of oscillation, $x(t)$, and the oscillation velocity, $u(t)$, were defined as follows:

$$x(t) = x_0 \sin(2\pi ft) \tag{3}$$

$$u(t) = 2\pi f x_0 \cos(2\pi ft) \tag{4}$$

However, at unsteady conditions the mass flow rate had to be used, expressed as:

$$\dot{m}(t) = \rho \cdot u(t) \cdot A \tag{5}$$

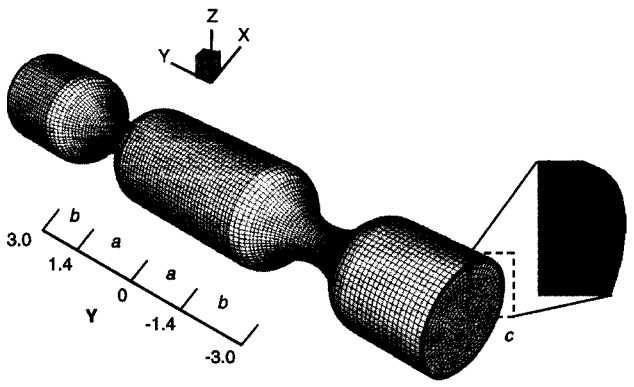

Figure 2. Mesh for 3D numerical simulations (units are radii of the tube, R). Details of mesh in zones a, b and c may be found in Table 2.

Table 2. Details of mesh used for 3D numerical simulations presented in Figure 2.

Mesh function	Meshing details
Axial mesh (zones a and b)	Linear spacing of 0.20 mm
Radial mesh (zone c)	Uniform boundary layer, 4 rows, growth factor of 1.2 meshed face: quad elements, map scheme, uniform spacing of 0.20 mm
Mesh volume (all zones)	Hex/wedge elements, cooper scheme, spacing of 0.20 mm with projected radial boundary layer along the axial distance total cells number: 110,772

where $u(t)$ is the velocity ($m\,s^{-1}$) and A is the cross-sectional area (m^2). For a 3D mesh, the cross-sectional area used was the cross-section of the mesh at the inlet/outlet point. For a 2D axisymmetric mesh, the cross-section was based on unit depth at the inlet.

The software did not allow the definition of unsteady inlet boundary conditions. This was overcome by discretising a sinusoidal oscillation cycle into many equal time steps, depending on the oscillation frequency (usually, 200 intervals per cycle). At each time step, the oscillation mass flow rate was introduced via a 'Fluent' journal file. Nonslip conditions were used as the wall boundary conditions. To ensure that the solution was independent of the initial conditions, the solver was allowed to run until the results were essentially the same from one oscillation to the next. The governing equations were solved sequentially using the segregated method solver. Underrelaxation was used to control the change of scalar variables in every iteration. The discretization scheme for pressure was second-order, and those for momentum and turbulence were second-order upwind schemes. The SIMPLEC algorithm was employed in the pressure-velocity coupling scheme.

Comparison of PIV and CFD Results

Qualitative analysis

A qualitative comparison of the two sets of data was performed by analysing the vortex behaviour, based on the vorticity, w, for a 2D flow, in the x–y plane (Perry, 2002):

$$w = \frac{1}{2}\left(\frac{\delta u_y}{\delta x} - \frac{\delta u_x}{\delta y}\right) \tag{6}$$

For PIV and 2D numerical simulations, all the points were coplanar, making the calculation of vorticity trivial. For 3D simulations, points on the x–y plane were selected and the calculation of w was made by the same method. However, since the flow in 3D simulations was expected to be nonaxisymmetric, it should be stated that the x–y plane is not necessarily representative of the vorticity in all other planes crossing the centre of the grid. The number, position and size of vortex rings were analysed, to allow the agreement between the experimental and computer-generated results to be assessed.

Vorticities were compared using the following procedure:

(1) values of w corresponding to points with y-coordinate between -6.5 and 6.5 mm were selected (i.e., one single cavity length)
(2) w values below 15% of the maximum vorticity in the centre of the cavity (straight zone) were filtered out for each time instant. Only the straight-walled section of the cavity was considered, as, due to the high curvature of the constriction and pronounced radial profiles of axial velocity, the higher w values near the constrictions and the walls of the cavity did not necessarily represent vortices
(3) the points where vorticity presents a local maximum/minimum were considered to be the centre of each vortex
(4) the size of each eddy was calculated by approximating the geometry of the filtered regions [from (2)] of each vortex to an elliptical shape and considering it to have a length, a, and a width, b. The vortex area could therefore be expressed as:

$$A_{vortex} = \frac{\pi \cdot a \cdot b}{4} \tag{7}$$

Quantitative analysis

To compare the results quantitatively, mixing intensity was calculated by quantifying the axial and radial velocities in the cavity, using an Excel spreadsheet. To compare the PIV results with the 2D numerical simulations, the axial and radial velocities in the x–y plane were used, but the velocity values in all the cells had to be used for the 3D mesh. The calculation was made for each velocity vector map (1/10 of an oscillation cycle), and the parameters determined using the follow procedures:

(1) *Instantaneous averaged (axial or radial) velocities* were determined by a mass balance across the surface (Perry, 2002):

$$\bar{u}(t) = \frac{1}{A}\int_A u(t)dA \tag{8}$$

where A is the flow cross-section. For the 2D axisymmetric grid, the cells are not of a uniform size, so the velocities were integrated in the axial and radial directions:

$$\bar{u}(t) = \frac{1}{A_{\text{total}}}\sum_{i=1}^{n}\sum_{j=1}^{m} u(t)_{ij} \cdot A_{ij} \tag{9}$$

where i and j represent the axial and radial components, respectively, $u(t)_{ij}$ is the component (radial or axial) of the velocity in the element of area, A_{ij}, and A_{total} is the total area of the cross-section, calculated by summing all the A_{ij} elements of the x–y plane. The cross-sectional area is presented by 'Fluent' as a 2D cell volume, i.e., the cross-section multiplied by π radians, and has area units. However, it should be noted that the value of averaged velocity in equation (9) is expressed

in relation to the mean diameter of the grid, i.e., about 3.82 mm ($d_{average}$) rather than 4.40 mm (d—diameter of the tube in the straight zone). Therefore, equation (9) must be multiplied by a factor of $(d_{average}/d)^2$ in order to obtain the average velocity expressed to the inlet cross section (with diameter d).

For the 3D grid, since cells in a specific plane (e.g., the $x-y$ plane) have different cross-sections and the cross-sectional areas of the cells were not available in 'Fluent', values of volume-averaged velocities were determined as follows:

$$\bar{u}(t) = \frac{1}{V_{total}} \sum_{i=1}^{n} \sum_{j=1}^{m} \sum_{k=1}^{p} u(t)_{ijk} . V_{ijk} \quad (10)$$

where $u(t)_{ijk}$ is the value of axial or radial velocity in the centre of the cell grid of unit volume V_{ijk} and V_{total} is the sum of all V_{ijk} elements. The average volume in equation (10) is again expressed in terms of the mean cross-section and the same factor as equation (9) must be used to calculate the average velocity in the straight zone (with diameter d).

(2) *Standard deviations,* σ of instantaneous area- or volume-averaged axial and radial velocities were calculated as follows:

$$\sigma(t) = \sqrt{\frac{\sum_{i=1}^{n} n_i \cdot u(t)_i^2}{N} - \bar{u}(t)^2} \quad (11)$$

where n_i is the height of the cross-sectional area or volume of the cell, i, and was determined by dividing the cross-section by the minimal cross-section of the 2D grid or, for the 3D mesh, as the ratio of the volume of each cell by the smallest cell volume in the grid. $u(t)$ is the velocity value in the cell, i, and $\bar{u}(t)$ is the area or volume-averaged velocity value at the time instant, t.

(3) *Average values of positive and negative components* were calculated at each time instant by the global value method presented in equations (9) and (10), by considering only the positive or negative velocity values. Again, the factor of $(d_{average}/d)^2$ must be used in order to express the area- or volume-averaged velocity components to the inlet cross section.

(4) *Full cycle average values* of axial and radial velocities were determined by averaging the values over a full cycle in the simulations, or over three oscillation cycles for the experimental PIV data, using equations (9) and (10). Full cycle standard deviations were determined using equation (11).

Particle and Bubble Suspension Experiments

When investigating the particle suspension performance of the screening mesoreactor, particles were injected at the top of the tube and oscillated until a steady concentration distribution was achieved. The three different kinds of particles used were: (a) ion exchange resin; (b) polyamine resin; and (c) silica resin. The particles' sedimentation velocities were determined by measuring the distance and time travelled by a particle in a 500 ml test tube, filled with water. The sedimentation velocities for particles (a)–(c) were 23.0, 1.5 and 2.5 mm s^{-1}, respectively. The silica resin and polyamine particles were in the size range 40–75 μm and the ion exchange resin particles were in the range 150–180 μm. A polyethylene fibre mesh was fitted to the bottom of the tube to prevent particles settling into the piston cavity when oscillation ceased. The volume fraction used in each set of experiments was determined by decreasing the fluid oscillations to specific conditions at which the particles sediment to the bottom of the tube. The height of the bed was then measured and the volume fraction expressed as the 'particle bed height/tube height $\times 100$'. The mass fraction was determined by drying the particles in a microwave oven and measuring the dry weight.

For bubble retention experiments, ~1 ml of air was injected through a syringe, under constant oscillation conditions, leading to the random formation of bubbles (i.e., mean size and size distributions of the bubbles were a function of the fluid oscillation conditions). Bubble suspension experiments were recorded visually at the centre of the tube, through the installed optical box, using a Samsung digital video camera at 25 frames per second, illuminated from above by a 50 W lamp.

RESULTS AND ANALYSES

Several PIV and CFD simulations were carried out at different combinations of fluid oscillation amplitudes and frequencies (for further details see section Materials and Methods). Observations across this range of conditions are reported here, but we have also focussed on a case study for the typical set of conditions: $Re_o = 348$, $x_0 = 1.1$ mm and $f = 11.1$ Hz.

Particle Image Velocimetry (PIV)

Experimental analysis of flow patterns within a single SPC tube and the effect of fluid oscillation conditions on fluid mixing were studied by PIV. In constricted tubes under oscillatory flow, two critical Re_os are usually used to represent obtained flow patterns: the first one (at a lower Re_o) is with the point at which flow separation occurs, and the second one (at a higher Re_o) represents the Re_o at which flow symmetry breaks.

In this study it was found that symmetrical eddy structures were in evidence at the lowest Re_os attainable with this oscillator unit ($Re_o = 12$, at $f = 2.1$ Hz, $x_0 = 0.2$). Therefore the lower critical Re_o is below this value.

The axisymmetry of the vortex rings was broken at approximately $Re_o = 100$ (when operating at $f = 1.1$ Hz; $x_0 = 3.8$ mm), leading to greater axial mixing. The dependence of the flow patterns on fluid oscillation amplitude was observed to differ from the dependence on oscillation frequency because the oscillation amplitude controls the eddy length detachment. This was also concluded by Ni *et al.* (1997) in studies on conventional larger OFRs with sharp-edged baffles, but conflicts with behaviour reported in further works (e.g., Ni and Pereira, 2000; Mackley and Ni, 1993). In the present study, flow patterns observed at similar Re_os (117 and 116), but at oscillation conditions of 4.1 Hz/1.0 mm and 1.1 Hz/3.8 mm, differ significantly: at high frequency, the eddy structures were generally

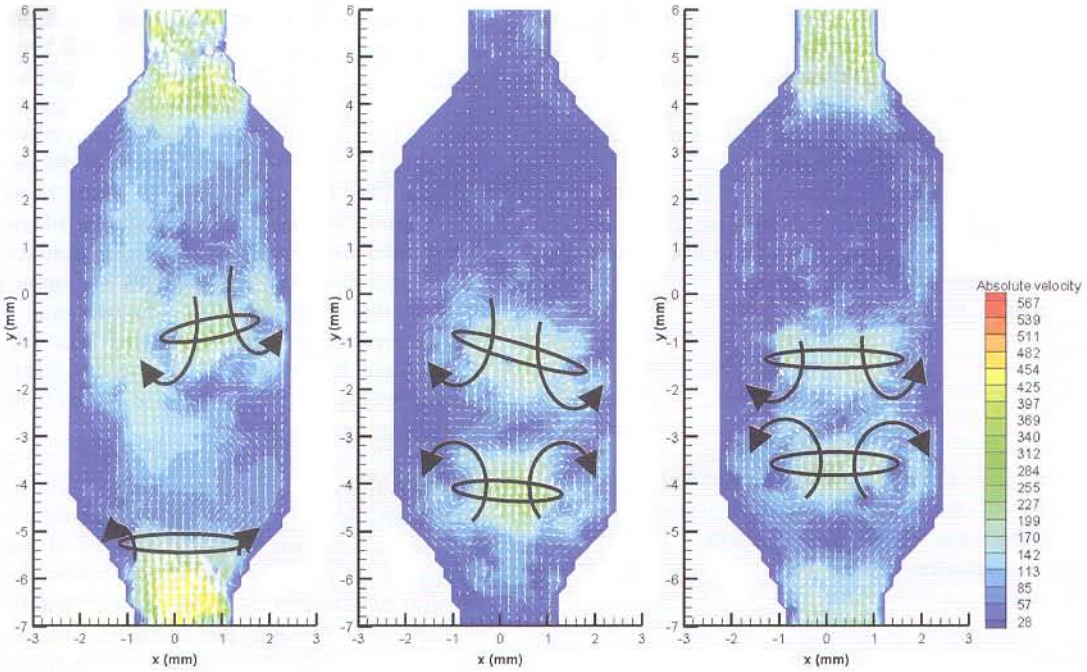

Figure 3. Instantaneous velocity vector maps at $Re_o = 348$, $x_0 = 1.1$ mm, $f = 11.1$ Hz coloured by absolute velocity magnitude (mm/s) and different phase angles (black vortex rings and arrows added to aid visualization): (a) beginning of cycle; (b) 1/5 way through cycle, i.e., before flow reversing; (c) 3/10 way through cycle, i.e., after flow reversing.

axisymmetrical, but at high amplitude axisymmetry was clearly broken at a Re_o near 100.

Typical observed flow patterns are shown in the instantaneous velocity vector maps in Figure 3 below, corresponding to three different points of the oscillation cycle:

(a) the point of maximum upward piston velocity (start of oscillation cycle);
(b) point of near-zero piston velocity (before flow reverses downwards);
(c) the point of minimum downward piston velocity, after flow reversal.

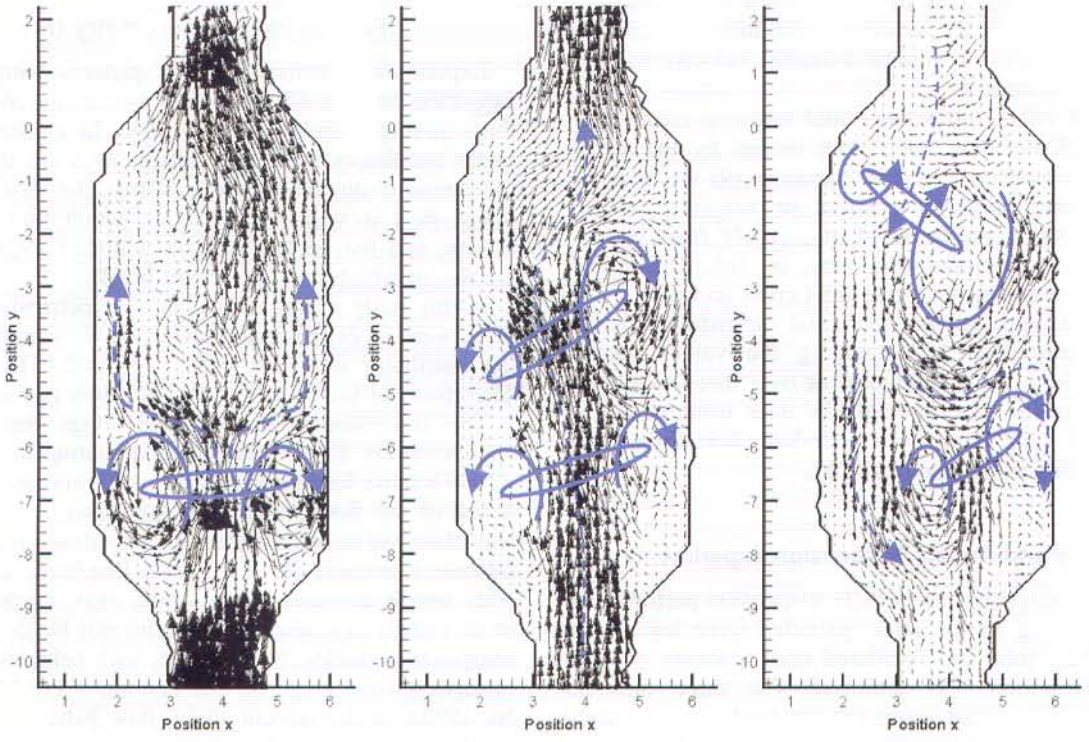

Figure 4. Instantaneous velocity vector maps at $Re_o = 1350$, $x_0 = 0.4$ mm, $f = 12.1$ Hz and different phase angles (blue vortex rings and arrows added to aid visualization): (a) start of a new cycle; (b) 1/5th way through cycle, i.e., before flow reversing; (c) 3/10th way through cycle, i.e., after flow reversing.

Table 3. Minimum critical Re_o observed for the screening reactor and comparison with some reported values for the conventional OFR.

Vortex rings geometry	Reactor mixing conditions	Screening reactor	Conventional OFR	
Axisymmetrical	Low axial mixing (or near plug flow behaviour at continuous flow)	$Re_o > 10$	$Re_o > 50$ $Re_o > 75$	Mackley and Ni, 1991 Mackley, 1990
Nonaxisymmetrical	Stirred tank behaviour	$Re_o > 100$	$Re_o > 300$ $Re_o > 400$	Howes *et al.*, 1991 Mackley, 1991

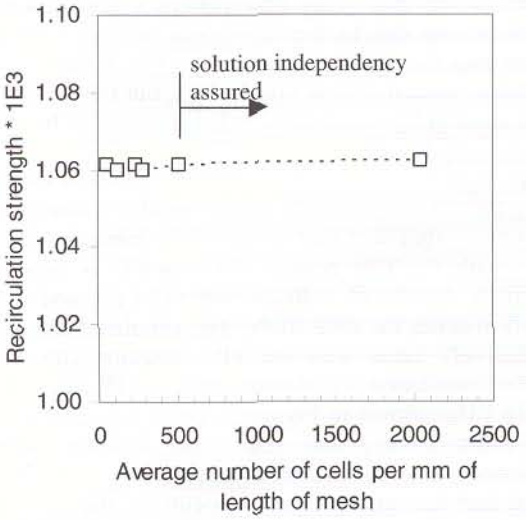

Figure 5a. (a) Influence of the grid size on the recirculation strength of steady state solution, $w_{max} - w_{wall}$, for continuous net flow, based on 2D planar model results ($Re = 100$).

The flow structures presented in Figure 3 may be interpreted as follows: at the lower constriction in Figure 3(a) there is flow separation, generating an upward-travelling vortex ring. The vortex ring emerges from the near-wall region and grows through Figures 3(b) and (c) to occupy most of the cross-sectional area of the tube, before colliding with the previous vortex ring. It should be noted that the nonaxisymmetry at the point of flow separation is related only to the nonaxisymmetric separation near the expansion (which is difficult to avoid in the tube's manufacture). Maximum nonaxisymmetry was observed in the velocity vector maps when $u(t)$ was near its maximum value (point a) of the oscillation cycle), while for points at lower axial velocities (e.g., in Figures 3(b) and (c), the vortex rings become more axisymmetric and more centrally located.

In Figure 3, the average residence time of each vortex ring was between 1.0 and 1.2 oscillation cycles. Each vortex ring was able to travel, on average, about half a cavity length. It should be noted that the point at which the vortex rings collide in Figure 3 is not in the middle.

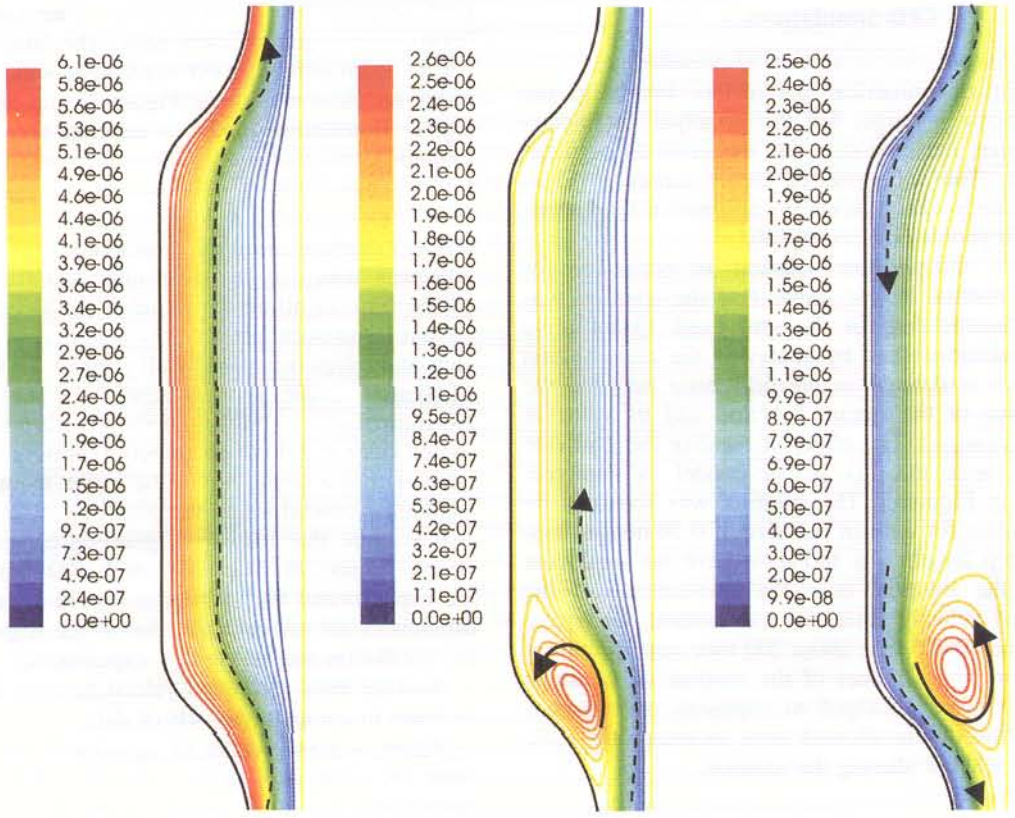

Figure 5b. (b) Simulated flow patterns for $Re_o = 11$, $x_0 = 0.2$ mm, $f = 2$ Hz, no net flow, using a 2D axisymmetric laminar model, after two simulation cycles. Contours of stream functions (kg s^{-1}) at: (a) start of cycle, i.e., maximum upward velocity; (b) 1/5 of an oscillation cycle, i.e., before flow reversing; (c) 3/10 of an oscillation cycle, i.e., after flow reversing.

This is due to slightly different velocities of the piston in the upward and downward directions. Apart from the initial asymmetry during flow separation, due to the asymmetry of the tube at the constriction, the mixing patterns observed in this reactor are essentially the same as those observed for larger, sharp-baffled OFRs. Therefore we can expect to achieve the same uniformity and efficiency of mixing, as well as particle suspension and bubble hold-up as has been observed in those reactors.

Figure 4, below, shows that the flow structures become considerably more asymmetrical at higher Re_os, as is the case in conventional OFRs. At $Re_o = 1350$, it is clear that symmetry is completely broken: it can be clearly seen that there are two vortex rings travelling in the same direction in Figure 4(b), and in Figure 4(c), we can see that although the rings are travelling in opposite directions they are highly asymmetrical. Clearly the SPC tube should not be operated at such high Re_os if plug flow is required, as there is a high degree of axial dispersion.

To ensure suspension of high concentrations of catalyst particles the oscillation frequencies must be increased, as intensive eddy structures will be required at *all phase angles*, as in Figure 4.

PIV analysis led to the conclusion that the critical Re_os for the screening reactor are lower than that for the conventional OFR. This is summarized in Table 3 below. Flow separation was observed at $Re_o \sim 10$ for the first case. This is approximately five times lower than the minimum value reported for the conventional OFR and is probably related to the greater constriction ratio of the SPC geometry.

CFD Simulations

Sensitivity of the solution to numerical parameters

The number of numerical parameters involving the numerical scheme is large, but the principal parameters are the grid size, the time-step and the error allowed for the velocities. The influence of these parameters was studied for a continuous flow (in the absence of fluid oscillations) at a Reynolds number of 100.

A grid size independent solution is necessary for validation of results. It was found that the solution was qualitatively independent of the grid used. Quantitative analysis was accomplished by analysing the recirculation strength, which is defined as the difference between the maximum value of the stream function and its value at the wall ($w_{max}-w_{wall}$). The effect of varying the grid size was checked with the 2D planar model is depicted, qualitatively, in Figure 5. The solution was found to be mesh-independent for a mean cell size of 0.20 mm or less.

The time-step length was found to have no significant influence on the solution, once the convergence of the momentum and velocity equations was assured. Its typical value was around 0.005, i.e., about 200 time steps per simulated oscillation cycle. Values of the residual in the range 0.001–0.0001 s were adjudged to represent convergence. Further reduction of the allowed error increased the CPU time required, without altering the solution.

Simulated flow patterns

Figure 6 shows the results of a 2D laminar axisymmetric model simulation at low axial mixing conditions ($Re_o = 11$), corresponding to conditions at which flow separation was observed by PIV.

Flow separation was not observed when $u(t)$ is at its maximum [Figure 5(a)], but when the following deceleration leads to formation of an eddy [Figure 5(b)]. Initially, flow is well-distributed radially, but as the axial velocity decreases, the flow moves preferentially to the centre of the tube. In Figure 5(c), as the flow then reverses, it instead passes along the walls, as the vortex ring moves to the centre of the tube. This flow pattern would ensure good radial mixing due to the movement of flow between the centre and the walls of the cavity. The vortex structures are not as intensive as at higher Re_os, but this demonstrates a mechanism by which good radial mixing can be achieved at relatively low Re_os.

The flow patterns produced by the numerical simulations using the 2D axisymmetric laminar model at low oscillation amplitudes (below 1 mm) generally exhibited good agreement with the PIV results. An example is presented in Figure 6, below, at a $Re_o = 348$ (11.1 Hz and 1.1 mm), which matches the case study. The simulated flow patterns qualitatively agree with the PIV measurements made at similar oscillation conditions ($Re_o = 348$, $x_0 = 1.1$ mm, $f = 11.1$ Hz) shown in Figure 3. There is vortex mixing in the entire cavity, and the 'wall flushing' effect of oscillatory flow can be clearly seen. Again, it should be stated that the mixing here is essentially the same as that occurring in larger, sharp-baffled, conventional OFRs.

To allow nonaxisymmetry to be simulated it was necessary to move to a 3D mesh. It was possible to simulate asymmetric flows using a laminar model, provided there were enough cells in the mesh, although simulation by LES required less computational time (as per Schlüter, 2000), as it required fewer cells. The laminar simulations below again exhibit good agreement with experimentally observed phenomena (see Figure 7) and are now able, in a three dimensional model, to generate non-axisymmetrical vortices.

Model matching using the case study

It was necessary to determine quantifiable properties of the flow to allow the simulations to be validated and ranked. One such property is the total vortex area. The sum of the area occupied by all vortices through a complete oscillation cycle is represented in Figure 8 below. No comparison with results from 2D planar model are presented since it did not accurately represent the fluid mechanics within a single SPC tube in the main range of fluid oscillation conditions in study.

It is clear that there is a good agreement between the vortex areas in the 3D and 2D simulations and the experimental PIV results. It should be noted that some differences are unavoidable, due to the imperfect action of the oscillation unit in the PIV experiments.

Average axial and radial velocities were also determined in order to compare the sets of data:

Again, a good degree of agreement was observed, for both the axial and radial velocities, indicating that the simulations are good models of the flow in the screening reactor. There is little difference between the 2D and 3D laminar simulations, although the 3D velocities are always slightly larger and therefore slightly closer to the

experimentally observed velocities. For low axial mixing conditions, i.e., a Re_o below 100, there was a complete agreement between the PIV results and the numerical simulations with the 2D axisymmetric laminar model in terms of location, number and size of vortices (results not shown here). At these oscillation conditions, the flow contains nonaxisymmetric vortex rings that the 2D axisymmetric model is inherently unable to simulate, but there is still semi-quantitative agreement with the PIV results, as the nonaxisymmetry is mild. In strongly nonaxisymmetric flows our evaluation criteria would show clear differences.

The numerical simulations helped to confirm that oscillation frequency affects the flow more significantly than the oscillation amplitude, because the use of small amplitudes leads to an increase in eddy intensity (smaller eddy size). Conversely, the use of high oscillation amplitudes increases the eddy size and decreases the number of visible eddy structures at any given phase angle of an oscillation cycle.

In the case study of Figures 6 and 7, the 2D axisymmetric simulations shown a better fit to the PIV data than results from planar simulations, as the size of eddy structures given by the planar model tend to be exaggerated and of too low an intensity. The 3D laminar model is an improvement as it is able to simulate nonaxisymmetry, but is very dependent on the mesh resolution.

No significant mesh dependence was observed for the 3D LES model. The results are in agreement with Ni *et al.* (2002), who claimed that the uniform mixing in an OFR is independent of turbulent intensity, and is instead due to 'laminar instabilities'. It was found that, due to the nature of the LES model, similar results to the 3D laminar model (with a fine mesh) may be achieved with lower CPU times.

The 2D axisymmetric model also exhibited better agreement with the vortex behaviour than the 3D laminar model (results not shown here). It is not clear why the number of simulated vortex rings is, on average, lower in the 3D modelling than in the experimental results, or why the total distance travelled by eddy structures is overestimated in the 3D modelling. The 2D axisymmetric model presents a good estimation of the vortex trail, but does not predict vortex dissipation time well. One explanation could be the existence of a tangential (swirl) flow, or the nonzero averaged axial velocity in the experimental data could be due to experimental error. The 2D axisymmetric model cannot simulate a tangential flow, but it is possible in the 3D laminar mode, but was not predicted (the averaged value of the tangential velocity component is also zero). It is difficult to say whether this result represents the true flow inside the SPC tube, or is a result of mesh dependency. The use of the periodic boundary layer in the numerical simulations should also be considered, as the flow patterns are constrained by the imposed periodicity of flow patterns in the next baffle cavity.

The comparison of the cycle average values (presented in Tables 4 and 5, following pages, based upon the data in Figures 9 and 10) for a Re_o of 388, $f = 11.1$ Hz and $x_0 = 1.1$ mm, demonstrates that simulation of the mixing intensity using the 3D laminar model is slightly closer to the experimental data than the results from the 2D axisymmetric simulations.

Particle and Bubble Suspensions

Effect of the concentration of particles

In order to investigate particle suspension in the screening mesoreactor, experiments were performed using three kinds of particles with distinct sizes and sedimentation velocities: silica resin, polyamine resin and ion exchange resin. Figure 11 below shows the relationship between the oscillation conditions and the maximum suspended concentration of ion exchange resin particles when the SPC tube was oriented vertically.

Note that the values shown in Figure 11 are expressed in terms of volume of particles per available internal volume of a SPC tube. For larger ion exchange resin particles these units were used because they were considered to accurately reflect the ion exchange resin particle suspension performance of the reactor, as this suspension represented a significant fraction of the available volume of the tube occupied. The maximum concentration of ion exchange resin particles (40% v/v, equivalent to 16% w/w) in well-mixed conditions was achieved at 12.1 Hz and 4 mm, with the SPC tube vertically oriented [Figure 11(a)]. Oscillation conditions at other combinations of amplitude and frequency (for a similar Re_o) were, unfortunately, impossible to achieve due to the limitations of the oscillator unit. Consequently, these were the most suitable oscillation conditions that could be achieved for suspension of such large particles.

It was found that it was easier to suspend particles at high frequencies and low amplitudes than at low frequencies and high amplitudes. This observation agrees with the findings of the PIV and is supported by Figure 11(b). The $u(t)_{max}$ required for complete suspension of particles (at constant particle concentration) exponentially decreases with the increase of f, approaching the value of sedimentation velocity of ion exchange resin particles (23.0 mm s^{-1}). When operating at low f (and consequently at high x_0), the $u(t)_{max}$ necessary for complete suspension of particles may be up to ten to fifteen times of the value of sedimentation velocity of particles, implying that the reactor has a lower energetic efficiency for particle suspension applications at these fluid oscillation conditions.

At the optimal oscillation conditions (12.1 Hz and 4 mm), it was also possible to keep 15% (w/w) of small diameter particles (polyamine particles) completely suspended within the SPC tube and to re-suspend these particles after settling within a few seconds.

PIV was conducted whilst catalyst particles were present. In Figure 12(a) and (b) below the flow structures are essentially unaffected by the presence of the catalyst particles, but in Figure 12(c) (at a different point in the oscillation) a certain degree of stratification of the particles has occurred, and has caused the flow to be pushed to one side of the tube. This may have to be taken into account in design of these reactors: that use of larger particles may necessitate increasing the axial dispersion of the flow.

Effect of reactor orientation on particle and bubble suspensions

In Figure 13, below, the suspension of ion exchange resin particles is shown for different angles of a SPC tube, between the horizontal (0°) and the vertical (90°). The oscillation conditions presented correspond to the

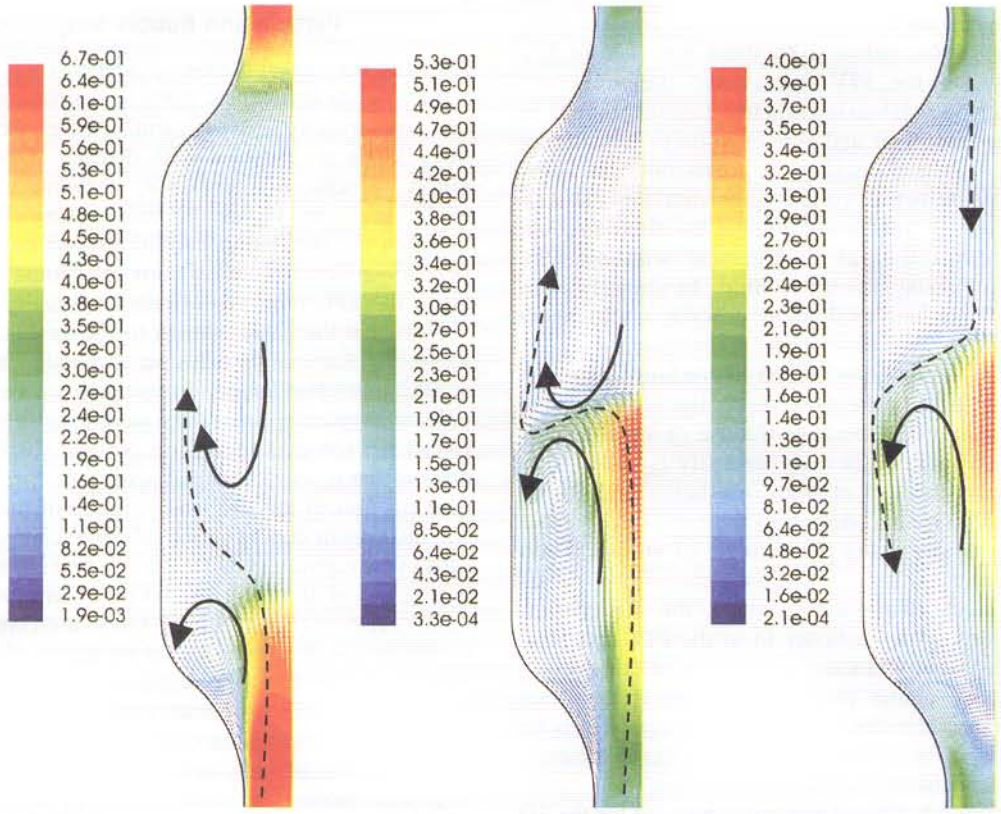

Figure 6. Simulated flow patterns for $Re_o = 348$, $x_0 = 1.1$ mm, $f = 11.1$ Hz, using a 2D axisymmetric laminar model, after 12 simulation cycles, no net flow. Velocity vectors coloured by velocity magnitude (m/s) at: (a) start of cycle, i.e., maximum upward velocity; (b) 1/5 of an oscillation cycle; (c) 3/10 of an oscillation cycle.

minimum necessary oscillation amplitude, at 12.1 Hz, to keep all the particles suspended. Ion exchange resin particles were used as they are relatively easy to observe, due to their relatively large particle diameter.

When SPC tube orientation was switched from vertical to horizontal, it was observed that it was easier to keep particles suspended when the reactor was in the horizontal rather than the vertical position. For example, at 12.1 Hz,

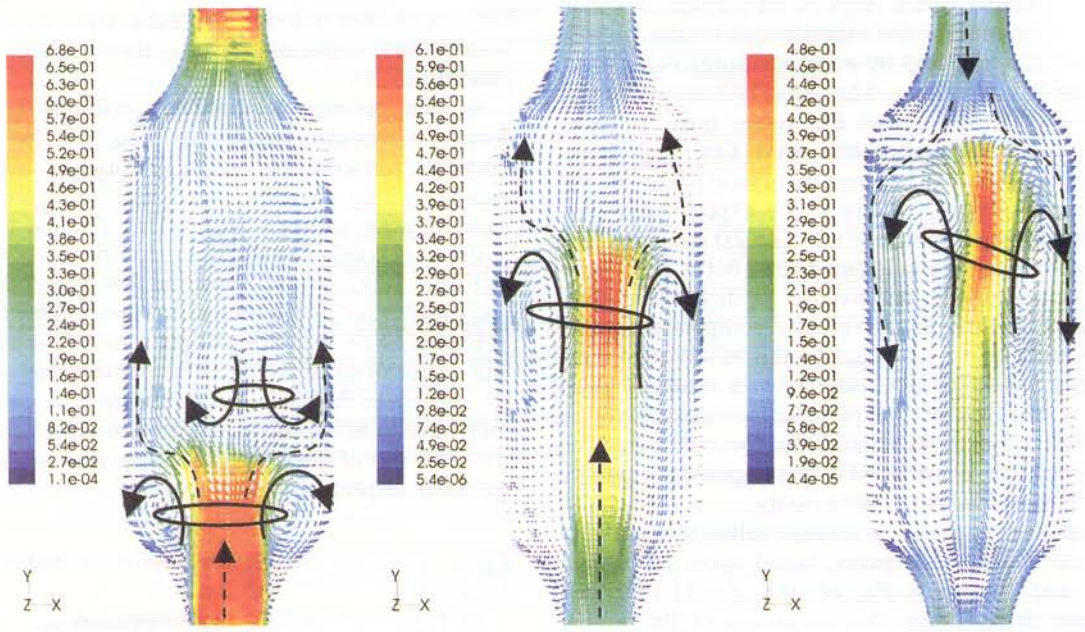

Figure 7. Simulated flow patterns for $Re_o = 348$, $x_0 = 1.1$ mm, $f = 11.1$ Hz, using a 3D laminar model, after 26 simulation cycles. Velocity vectors coloured by velocity magnitude (m/s), on plane $z = 0$, (black arrows added to aid visualization) at: (a) start of cycle, i.e., maximum upward velocity; (b) 1/5 of an oscillation cycle, i.e., before flow reversing; (c) 3/10 of an oscillation cycle, i.e., after flow reversing.

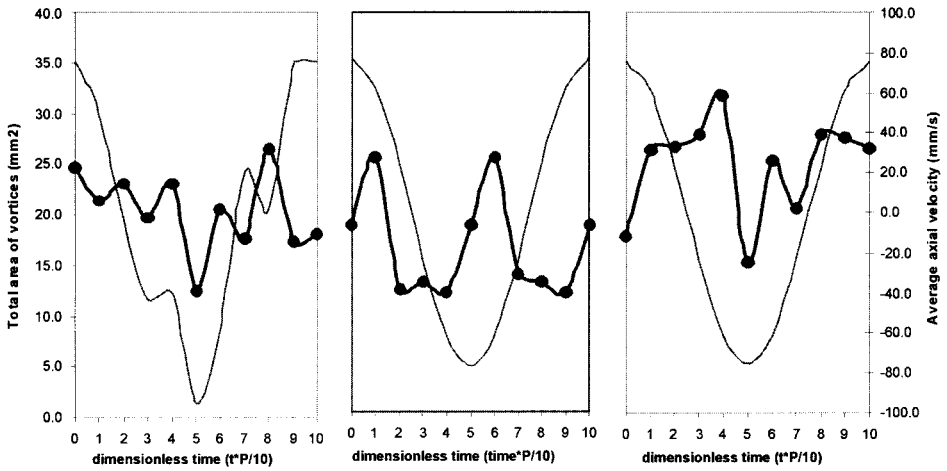

Figure 8. Comparison of the total areas occupied by the vortices (•) in different instants of the oscillation cycle ($Re_o = 348$, $x_0 = 1.1$ mm, $f = 11.1$ Hz; no net flow, i.e., $Re_n = 0$) for: (a) experimental PIV data; (b) 2D axisymmetric laminar numerical simulations; (c) 3D laminar numerical simulations.

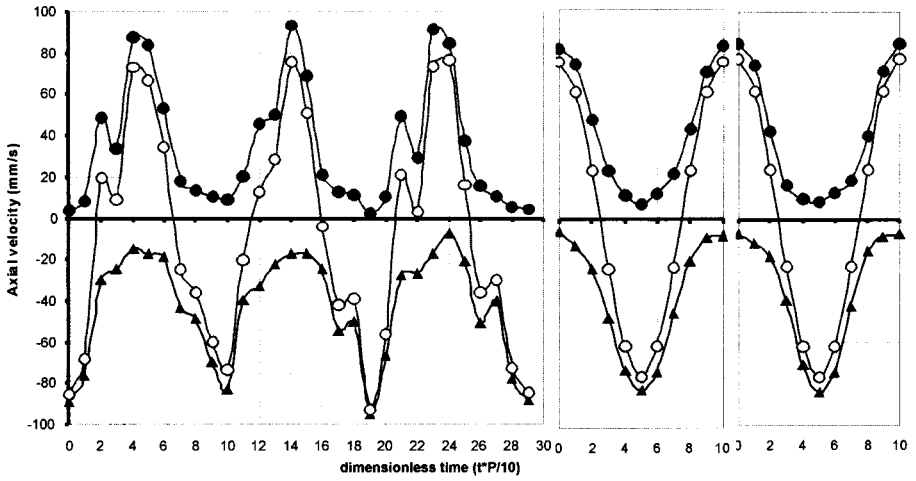

Figure 9. Average of axial velocities through the oscillation cycle at $Re_o = 348$, $f = 12.1$ Hz, $x_0 = 1.2$ mm, using (a) experimental data from PIV; (b) data from numerical modelling using a 2D laminar axisymmetric model; and (c) data from numerical modelling using a 3D laminar model. (○) global averaged axial velocity; (•) average of positive values of axial velocity; (▲) average of negative values of axial velocities.

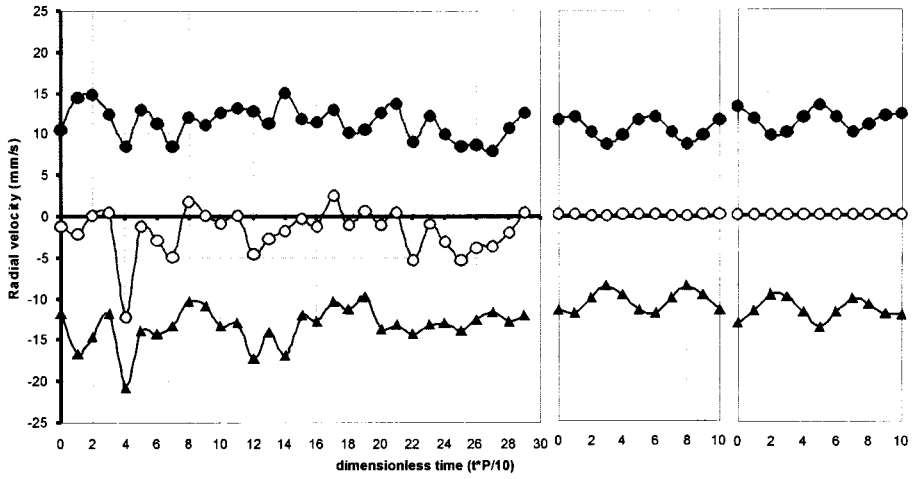

Figure 10. Average of radial velocities through the oscillation cycle using (a) experimental data from PIV; (b) data from numerical modelling using a 2D laminar axisymmetric model; and (c) data from numerical modelling using a 3D laminar model using cells at plane $z = 0$. (○) global averaged radial velocity; (•) average of positive values of radial velocity; (▲) average of negative values of radial velocities. Connection lines just intend to represent a tendency. $Re_o = 348$; $f = 12.1$ Hz, $x_0 = 1.2$ mm.

Table 4. Comparison of cycle average axial, radial (and tangential) velocities measured by PIV with the results from numerical simulations, using 2D axisymmetric and 3D laminar models; $Re_o = 348, f = 11.1$ Hz, $x_0 = 1.1$. $Re_n = 0$.

		Axial velocity (mm s^{-1})			Radial velocity (mm s^{-1})			Tangential velocity (mm s^{-1})		
		Global	V^+_{axial}	V^-_{axial}	Global	V^+_{radial}	V^-_{radial}	Global	V^+_{tang}	V^-_{tang}
Without flow reversing[1]	Average	0.0	24.4	−24.4	—	—	—	—	—	—
	σ	54.5	—	—	—	—	—	—	—	—
	Min	−76.7	—	—	—	—	—	—	—	—
	Max	76.7	—	—	—	—	—	—	—	—
Experimental PIV	Average	−8.8	34.4	−43.2	−1.9	11.5	−13.3	—	—	—
	σ	115.2	—	—	37.2	—	—	—	—	—
	Min	−595.6	—	—	−321.9	—	—	—	—	—
	Max	539.6	—	—	90.1	—	—	—	—	—
2D axisymmetric laminar model	Average	0.0	37.5	−37.5	0.0	10.5	−10.4	—	—	—
	σ	105.6	—	—	32.2	—	—	—	—	—
	Min	−668.2	—	—	−136.7	—	—	—	—	—
	Max	668.2	—	—	256.3	—	—	—	—	—
3D laminar model	Average	0.0	39.3	−39.3	−0.01	11.5	−11.5	−0.0	9.9	−9.9
	σ	112.9	—	—	33.2	—	—	29.1	—	—
	Min	−681.5	—	—	−318.0	—	—	−346.6	—	—
	Max	679.3	—	—	358.4	—	—	285.3	—	—

[1]Assuming fluid oscillated at same oscillation conditions in a smooth pipe.

an amplitude of 3 mm is enough to keep 40% (v/v) of ion exchange resin particles completely suspended with the tube positioned horizontally, but an oscillation amplitude of 4 mm is needed to keep the same quantity of particles completely suspended when the tube is held vertically. This means a considerable decrease on the required power input to keep the same amount of particles completely suspended with the swap of tube orientation from the vertical to the horizontal position. This may be due to differences of pressure drop between the two situations: when the SPC tube is positioned vertically, the particles in the bottom are at a higher static pressure than those at the top of the tube, due to the height of the particle 'bed'. Thus, a higher power input is required in order to suspend the same amount of particles.

Bubble retention

Due to the small scale of the SPC geometry the problem of gas washout must be considered during reactor design. Therefore, the effect of reactor angle on bubble washout was investigated, at the optimal oscillation conditions given above (a frequency of 12.1 Hz and an amplitude between 3 mm and 4 mm, depending on the tube orientation). It was observed that the screening reactor had a self-cleaning capacity at angles above 45° at batch mode, i.e. washout of bubbles naturally occurs at tube orientations above 45° thus gas retention in the cavities is avoided. At smaller angles (near horizontal) small diameter (<1.6 mm) bubbles were retained inside each cavity. The washout of these small diameter bubbles is the most important parameter in determining the reactor's angle.

In practise, an angle smaller than 45° will allow reactor tubes to be arranged in series (Figure 14). Thus, the optimal minimum angle for the reactor was determined to be 10°. This position does not limit the natural washout of large (>1.6 mm) bubbles (even in batch mode), and may be a useful result, if the screening reactor is operated at low bubble breakage conditions. If a high power input is required (which may lead to significant bubble breakage) the small bubbles can be cleaned from the system by imposing a cyclic net flow of 14 ml/min (corresponding to a residence time of 20 s) for less than one minute, per SPC tube.

A significant increase in the mean residence time of the bubbles was observed when the fluid was oscillated at the optimal conditions (12 Hz and 4 mm), even when the tube was positioned vertically. This means that the operation of SPC tube under oscillatory conditions may lead to higher bubble contact time, which has the potential to enhance mass transfer processes, such as air-water oxygen mass transfer coefficient.

Table 5. Comparison of measured mixing intensity by PIV with the results from numerical simulations, using 2D axisymmetric and 3D laminar models; $Re_o = 348, f = 11.1$ Hz, $x_0 = 1.1$ mm

	Average ratio V_{radial}/V_{axial}	Averaged axial circulation rate (mm s^{-1})	Predicted mixing time (s)
PIV	0.32	0.59	0.25
2D axisymmetric laminar model	0.28	0.57	0.26
3D laminar model	0.29	0.60	0.25
STR[1]	—	0.02	3.65

[1]Data from Rase (1977), assuming a STR with same d/L ratio as a single SPC cavity.

CONCLUSIONS AND DISCUSSION

This paper has presented PIV data for a millimetre-scale oscillatory flow screening mesoreactor geometry with smooth periodic constrictions. The results demonstrate that the mixing previously observed at larger scales (e.g., in 'conventional' oscillatory flow), with sharp baffles, can be reproduced at this, smaller scale in a reactor with

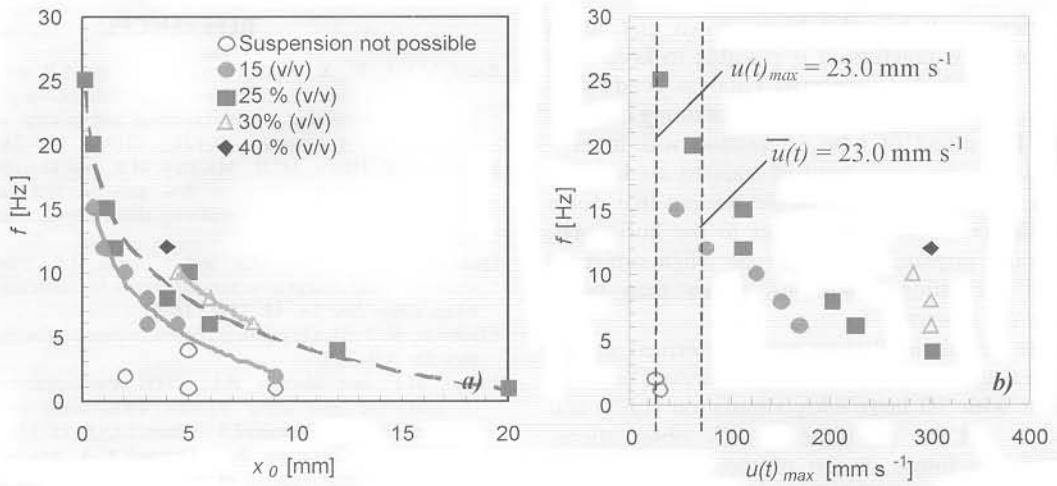

Figure 11. (a) Maximum concentration of ion exchange resin particles completely suspended at different fluid oscillations frequencies and amplitudes for a vertically fixed SPC tube; (b) minimum $u(t)_{max}$ (maximum oscillation velocities) for complete suspension of particles, at different fluid oscillation frequencies.

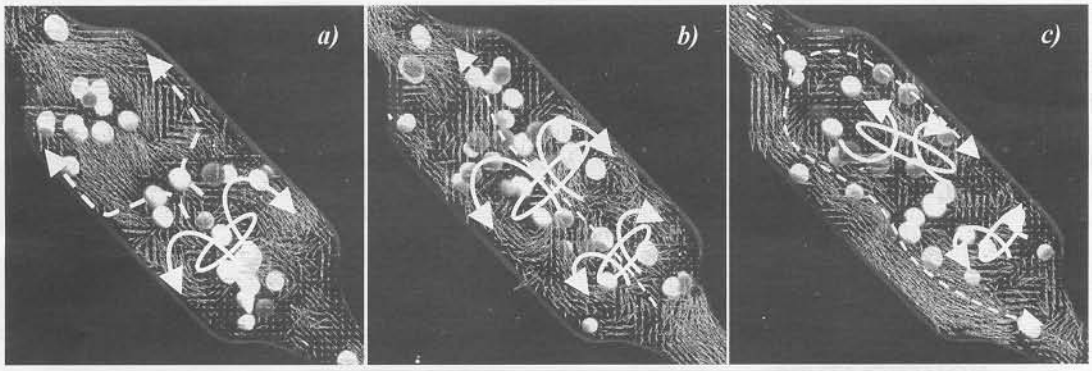

Figure 12. Instantaneous velocity vector maps of fluid phase at $Re_o = 990$, $x_0 = 3$ mm, $f = 12.1$ Hz and 45° of tube position in the presence of a small amount of ion exchange resin particles: (a) start of a new cycle; (b) 1/5 way through cycle, i.e., before flow reversing; (c) 3/10 way through cycle, i.e., after flow reversing. $Re_n = 0$. White arrows added to aid visualization. Top of images corresponds to the bottom of the cavity.

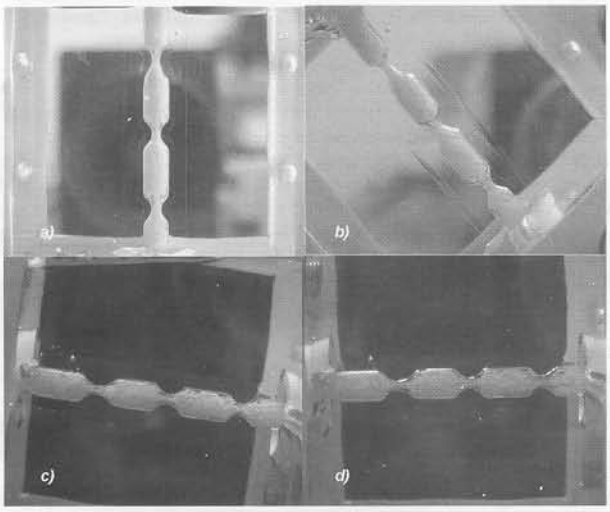

Figure 13. Complete suspension of 40% v/v of ion exchange resin particles at varying angles and similar oscillation conditions: (a) vertical position, $f = 12.1$ Hz, $x_0 = 4$ mm; (b) 45°, $f = 12.1$ Hz, $x_0 = 4$ mm; (c) 10°, $f = 12.1$ Hz, $x_0 = 3$ mm; (d) horizontal position, $f = 12.1$ Hz, $x_0 = 3$ mm. In (b), (c) and (d), the right-hand side corresponds to the bottom of the tube.

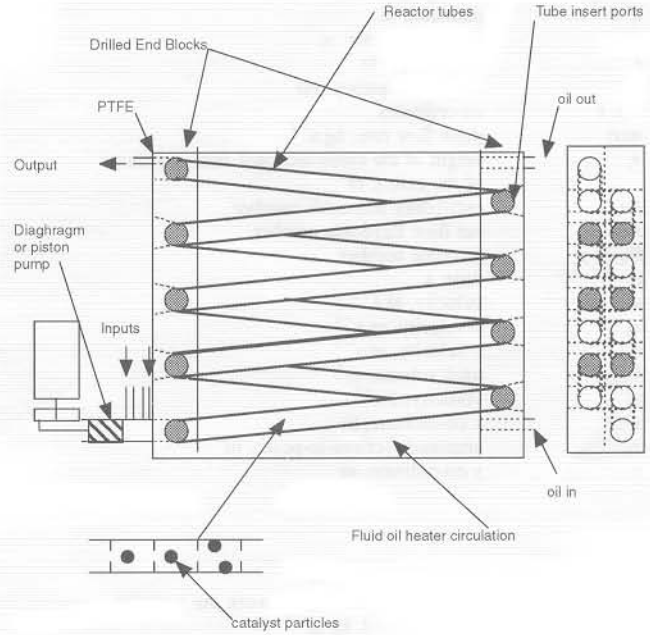

Figure 14. Proposed 'in series' configuration for a single screening reactor unit.

smooth constrictions. It has also been shown that, as in larger oscillatory flow reactors, it is possible to keep high concentrations of polymer-supported catalyst beads suspended in the screening reactor, whilst maintaining uniform fluid mixing. The effect of tube orientation was investigated in relation to the movement of trapped air bubbles within the reactor tube, resulting in the finding that, for a tube oriented at ten degrees or greater to the horizontal, air bubbles would migrate along the tube when subjected to appropriate oscillation conditions, rather than being trapped within the reactor.

Matching numerical simulations were performed and, in general, a high degree of correlation was observed between the simulations with 3D large eddy simulation (LES) and laminar models and the experimental PIV observations. This should aid in future design of these reactors. For reactors which operate at a Re_o below 100, a simple 2D axisymmetric laminar simulation will fully describe the flow, and for most aspects of design will be good enough for higher Re_os (up to 1200).

The data presented here is the basis for a concept design of a continuous small-scale reactor, to be used in speciality chemicals manufacture and high-throughput screening. A schematic of a prototype is shown in Figure 14. The reactor will have the capability to perform sequential reactions, by keeping different solid particles or reactants in separate tubes. A significant advantage of the system is that the mixing conditions achieved in the laboratory can easily be achieved at larger scales (Stonestreet and Harvey, 2002), as scale-up is predictable.

NOMENCLATURE

A_{ij}	area of element, m^2
A_{total}	cross-sectional area, m^2
A_{vortex}	vortex area, m^2
B	particle weight percentage, %
$d_{average}$	average diameter, m
d	diameter, m
d_0	orifice diameter, m
f	frequency, Hz
f_c	critical frequency, Hz
i, j, k	co-ordinates
$m(t)$	mass flow rate, kg s^{-1}
n_i	height of the cross-sectional area or volume of the cell, i, m
Re_o	oscillatory Reynolds number
Re_n	net flow Reynolds number
St_r	Strouhal number
t	time, s
$u(t)$	velocity, m s^{-1}
u_y	y-velocity, m s^{-1}
u_x	x-velocity, m s^{-1}
V_{total}	total volume, m^3
w	vorticity, 1 s^{-1}
x	x co-ordinate, m
x_0	amplitude (centre-to-peak), m
y	y co-ordinate, m

Greek letters

ρ	liquid density, kg m^{-3}
$\Delta\rho$	difference of density between the particles and the liquid, kg m^{-3}
μ	viscosity, kg m^{-1} s^{-1}
σ	standard deviation
ν	kinematic viscosity, m^2 s^{-1}

REFERENCES

Baird, M.H.I., Ni, X., Mackley, M.R., Harvey, A.P. and Stonestreet, P., 2003, Mixing through oscillations and pulsations – a guide to achieving process enhancements in the chemical and process industries, *Trans IChemE, Part A, Chem Eng Res Des*, 81(A3): 373–383.

Brunold, C.R., Hunns, J.C.B., Mackley, M.R. and Thompson, J.W., 1989, Experimental-observations on flow patterns and energy-losses for oscillatory flow in ducts containing sharp edges, *Chem Eng Sci*, 44: 1227–1244.

Dickens, A.W., Mackley, M.R. and Williams, H.R., 1989, Experimental residence time distribution measurements for unsteady-flow in baffled tubes, *Chem Eng Sci*, 44: 1471–1479.

Elgobashi, S., 1994, On prediction particle-laden turbulent flows, *App Sci Res*, 52: 309–329.

Fabiyi, M.E. and Skelton, R.L., 2000, Photocatalytic mineralisation of methylene blue using buoyant TiO_2-coated polystyrene beads. *J Photochem and Photobiol A—Chem*, 132(1–2): 121–128.

Gao, S., Ni, X., Cumming, R.H., Greated, C.A. and Norman, P., 1998, Experimental investigation of bentonite flocculation in a batch oscillatory baffled column, *Separ Sci Technol*, 33: 2143–2157.

Hewgill, M.R., Mackley, M.R., Pandit, A.B. and Pannu, S.S., 1993, Enhancement of gas-liquid mass-transfer using oscillatory flow in a baffled tube, *Chem Eng Sci*, 48: 799–809.

Howes, T., 1988, *On the Dispersion of Unsteady Flow in Baffled Tubes*, PhD thesis, Department of Chemical Engineering, Cambridge University, Cambridge, UK.

Howes, T. and Mackley, M.R., 1990, Experimental axial-dispersion for oscillatory flow through a baffled tube, *Chem Eng Sci*, 45: 1349–1358.

Howes, T., Mackley, M.R. and Roberts, E.P.L., 1991, The simulation of chaotic mixing and dispersion for periodic flows in baffled channels, *Chem Eng Sci*, 46: 1669–1677.

Liu, S., Ni, X., Greated, C.A. and Fryer, P.J., 1995, Measurements of velocities of single particles for steady and oscillatory flows in plain and baffled tubes, *Trans IChemE, Part A, Chem Eng Res Des*, 73: 727–732.

Mackley, M.R., 1991, Process innovation using oscillatory flow within baffled tubes, *Trans IChemE, Part A, Chem Eng Res Des*, 69: 197–199.

Mackley, M.R., Tweddle, G.M. and Wyatt, I.D., 1990, Experimental heat-transfer measurements for pulsatile flow in baffled tubes, *Chem Eng Sci*, 45: 1237–1242.

Mackley, M.R. and Ni, X., 1991, Mixing and dispersion in a baffled tube for steady laminar and pulsatile flow, *Chem Eng Sci*, 46: 3139–3151.

Mackley, M.R. and Ni, X., 1993, Experimental fluid dispersion measurements in periodic baffled tube arrays, *Chem Eng Sci*, 48: 3293–3305.

Mackley, M.R., Smith, K.B. and Wise, N.P., 1993, The mixing and separation of particle suspensions using oscillatory flow in baffled tubes, *Trans IChemE, Part A, Chem Eng Res Des*, 71: 649–656.

Mackley, M.R. and Stonestreet, P., 1995, Heat-transfer and associated energy-dissipation for oscillatory flow in baffled tubes, *Chem Eng Sci*, 50: 2211–2224.

Ni, X.W., 1994, Residence time distribution measurements in a pulsed baffled tube bundle, *J Chem Technol Biot*, 59: 213–221.

Ni, X. and Mackley, M.R., 1993, Chemical-reaction in batch pulsatile flow and stirred-tank reactors, *Chem Eng J Bioch Eng*, 52: 107–114.

Ni, X.W., Gao, S.W. and Pritchard, D.W., 1995a, Study of mass-transfer in yeast in a pulsed baffled bioreactor, *Biotechnol Bioeng*, 45: 165–175.

Ni, X., Gao, S., Cumming, R.H. and Pritchard, D.W., 1995b, A comparative-study of mass-transfer in yeast for a batch pulsed baffled bioreactor and a stirred-tank fermenter, *Chem Eng Sci*, 50: 2127–2136.

Ni, X., Liu, S., Grewal, P.S. and Greated, C.A., 1995c, A study of velocity vector profile and strain rate distribution for laminar and oscillatory flows in a baffled tube using particle imaging velocimetry, *J Flow Visual Image Proc*, 2: 135–147.

Ni, X. and Gao, S., 1996, Scale-up correlation for mass transfercoefficients in pulsed baffled reactors, *J Chem Eng*, 63: 157–166.

Ni, X. and Gough, P., 1997, On the discussion of the dimensionless groups governing oscillatory flow in a baffled tube, *Chem Eng Sci*, 52: 3209–3212.

Ni, X., Zhang, Y. and Mustafa, I., 1998, An investigation of droplet size and size distribution in methylmethacrylate suspensions in a batch oscillatory-baffled reactor, *Chem Eng Sci*, 53: 2903–2919.

Ni, X., Zhang, Y. and Mustafa, I., 1999, Correlation of polymer particle size with droplet size in suspension polymerisation of methylmethacrylate in a batch oscillatory-baffled reactor, *Chem Eng Sci*, 54: 841–850.

Ni, X.W. and Pereira, N.E., 2000, Parameters affecting fluid dispersion in a continuous oscillatory baffled tube, *J AIChE*, 46: 37–45.

Ni, X., Jian, H. and Fitch, A.W., 2002, Computational fluid dynamic modelling of flow patterns in an oscillatory baffled column, *Chem Eng Sci*, 57: 2849–2862.

Perry, R.P., Green, D.W. and Maloney, J.O., 2002, *Perry's Chemicals Engineer*, Platinum edition (McGraw-Hill, New York, USA).

Rase, H.F., 1977, *Chemical Reactor Design for Process Plants, Volume One: Principles and Techniques* (Wiley-Interscience, New York, USA).

Schlüter, J.U., 2000, *Large Eddy Simulations of flow and mixing in jets and swirl flows: applications to gas turbines*, PhD thesis, CERFACS, Toulousse, France.

Smith, K.B., 1999, *The scale-up of oscillatory flow mixing*, PhD Thesis, University of Cambridge, UK.

Stonestreet, P. and Harvey, A.P., 2002, A mixing-based design methodology for continuous oscillatory flow reactors, *Trans IChemE, Part A, Chem Eng Res Des*, 80: 31–44.

Stonestreet, P. and van der Veeken, P.M.J., 1999, The effects of oscillatory flow and bulk flow components on the residence time distribution in baffled tube reactors. *Trans IChemE, Part A, Chem Eng Res Des*, 77: 671–684.

ACKNOWLEDGEMENTS

Nuno Reis would like to thank Fundação da Ciência e Tecnologia, Portugal, for the scholarship SFRH/BD/6954/2001. Adam Harvey would like to thank the EPSRC for financial support.

The manuscript was received 20 November 2003 and accepted for publication after revision 23 December 2004.